

Application of Multiple Scattering Theory to Lower Energy Elastic Nucleon-Nucleus Reactions

C.R. Chinn^{(a),(b)}, Ch. Elster^(c), R.M. Thaler^{(a),(d)}, and S.P. Weppner^(c)

^(a) *Department of Physics and Astronomy, Vanderbilt University, Nashville, TN 37235*

^(b) *Center for Computationally Intensive Physics*

Oak Ridge National Laboratory, Oak Ridge, TN 37831-6373

^(c) *Institute of Nuclear and Particle Physics, and Department of Physics,*

Ohio University, Athens, OH 45701

^(d) *Physics Department, Case Western Reserve University, Cleveland, OH 44106.*

(June 30, 2021)

PACS: 25.40.Cm

Typeset using REVTeX

Abstract

The optical model potentials for nucleon-nucleus elastic scattering at 65 MeV are calculated for ^{12}C , ^{16}O , ^{28}Si , ^{40}Ca , ^{56}Fe , ^{90}Zr and ^{208}Pb in first order multiple scattering theory, following the prescription of the spectator expansion, where the only inputs are the free NN potentials, the nuclear densities and the nuclear mean field as derived from microscopic nuclear structure calculations. These potentials are used to predict differential cross sections, analyzing powers and spin rotation functions for neutron and proton scattering at 65 MeV projectile energy and compared with available experimental data. The theoretical curves are in surprisingly good agreement with the data. The modification of the propagator due to the coupling of the struck nucleon to the residual nucleus is seen to be significant at this energy and invariably improves the congruence of theoretical prediction and measurement.

I. INTRODUCTION

Recently measurements of 65 MeV neutron-nucleus elastic differential cross sections have been published [1]. Together with the corresponding proton data, one now has an opportunity to study the effects of isospin degrees of freedom and to analyze multiple scattering theory with and without the coulomb field at low energies. In the past it had been assumed that first order multiple scattering theory would prove unable to provide an accurate representation of experiments at such low energies and thus models in the form of phenomenological optical potentials or effective nucleon-nucleon interactions were proposed. With recent advances in our ability to calculate the first term in a multiple scattering expansion together with the influence of the mean field potential binding the struck nucleon to the target nucleus, it is now possible to test whether one is able to represent low-energy scattering in the first order or whether one must consider higher order scattering terms, all within a parameter-free description.

II. FORMALISM

We have been pursuing a program of calculation of elastic nucleon-nucleus scattering at energies sufficiently high such that first order multiple scattering theory in the forward cone provides a good description of the data [2,3]. In this program the only inputs are the nucleon-nucleon (NN) interaction, represented by NN t-matrices, the target wave functions, and the static target nuclear mean field. These quantities are incorporated into multiple scattering theory in the hierarchical spectator expansion for the optical potential, in which the transition operator, T , is defined to be

$$T = U + UG_0PT. \tag{2.1}$$

The operator P is the projector onto the target initial state. The optical potential operator U is given in the spectator expansion as:

$$U = \sum_i \tau_i + \sum_{i,j \neq i} \tau_{ij} + \dots \quad (2.2)$$

The first order theory corresponds to a truncation of this series to a single term,

$$U \approx \sum_i \tau_i, \quad (2.3)$$

where

$$\tau_i = v_{0i} + v_{0i} G_0 (1 - P) \tau_i \quad (2.4)$$

Here v_{0i} stands for the potential between the projectile nucleon (0) and the i th target nucleon. The propagator G_0 is given by

$$\begin{aligned} G_0^{-1} &= E - h_0 - H_A \\ &= E - h_0 - h_i - \sum_{j \neq i} v_{ij} - H^i \\ &= E - h_0 - H_i - H^i, \end{aligned} \quad (2.5)$$

where h_i is the kinetic energy operator for nucleon i and $H_A = H_i + H^i$ is the target Hamiltonian. The operator, τ_i , can be reexpressed in a solvable one-body integral equation as

$$\tau_i = \tilde{t}_{0i} - \tilde{t}_{0i} G_0 P \tau_i, \quad (2.6)$$

where \tilde{t}_{0i} is given to be:

$$\begin{aligned} \tilde{t}_{0i} &= t_{0i}^{free} + t_{0i}^{free} [G_0 - g_0] \tilde{t}_{0i} \\ &= t_{0i}^{free} + t_{0i}^{free} g_0 \mathcal{T}_i g_0 \tilde{t}_{0i}. \end{aligned} \quad (2.7)$$

Here t_{0i}^{free} is the free NN t-matrix and g_0 is the free NN propagator for the active pair consisting of projectile and target nucleon $[g_0^{-1} = E' - h_0 - h_i]$. The scattering operator \mathcal{T}_i expresses the scattering of the target nucleon (i) from the residual nucleus, which is represented by $\sum_{j \neq i} v_{ij}$. The explicit treatment of Eq. (2.7) is described in detail in Ref. [2] and is directly derivable within the spectator expansion of multiple scattering theory. The

right term of Eq. (2.7) results from the difference between the free propagator g_0 with G_0 , which corresponds to the propagation of the target nucleon through the nuclear medium and can be thought of as a propagator modification.

The first order optical potential is then constructed with the operator, τ_i , from Eq. (2.6):

$$U_{opt} = \langle \vec{k}'_0 \Psi_A | \sum_i \tau_i | \vec{k}_0 \Psi_A \rangle . \quad (2.8)$$

In the present calculations, which are performed in momentum space, U_{opt} enters in the ‘optimum factorized’ or ‘off-shell $\tau\rho$ ’ form as

$$U_{opt} \approx \tau(q, \mathcal{K}; E) \rho(q) , \quad (2.9)$$

where $q = k'_0 - k_0$ and $\mathcal{K} = \frac{1}{2}(k'_0 + k_0)$; k'_0 and k_0 are the final and initial momenta of the projectile. This corresponds to a steepest descent evaluation of the ‘full-folding’ integral, in which the τ is convoluted with the nonlocal density as indicated schematically in Eq. (2.8). For harmonic oscillator model densities it has been shown that the optimum factorized form represents the nonlocal character of U_{opt} qualitatively in the intermediate energy regime [4,5]. Complete ‘full-folding’ calculations with more realistic nuclear densities are in progress. It is to be understood that all spin summations are performed in obtaining U_{opt} (under the usual assumption of a spin-saturated target), thus reducing the required NN t-matrix elements to the spin-independent component (corresponding to the Wolfenstein amplitude A) and the spin-orbit component (corresponding to the Wolfenstein amplitude C). All scattering calculations presented here contain an additional factor in the optical potential to account for the transformation of the NN t-matrix from the two-nucleon c.m. frame to the nucleon-nucleus c.m. frame [6].

III. THEORETICAL PREDICTIONS

For a calculation of the first order optical potential in the optimum factorized form, the quantities $\tau(q, \mathcal{K}; E)$ and $\rho(q)$ are required as input. All calculations presented

in this paper are based on the full Bonn Potential [7] as the NN interaction from which $\tau(q, \mathcal{K}; E)$ is obtained. As can be seen from Eq. (2.6), the quantity $(\tau\rho)$ can be calculated as the solution of a one-body integral equation in which $(\tilde{t}\rho)$ serves as the driving term. The proton densities are taken from charge densities measured in electron scattering experiments [12]. Although the neutron distribution in nuclei are not completely determined by measurement, nuclear structure calculations indicate significant differences between the proton and neutron distributions. These differences are nonnegligible in our reaction calculations and especially affect the location of the diffraction minima and become even more pronounced in the case of neutron scattering. We believe neutron densities taken from the Hartree-Fock-Bogolyubov calculations of Ref. [8] give the best presently available representation of the neutron distributions. These are the densities used in the present work.

The calculation of \tilde{t}_{0i} according to Eq. (2.7) requires the free NN t-matrix as well as \mathcal{T}_i , the ‘t-matrix’ representing the scattering of the struck target nucleon from the residual nucleus. A one-body mean field potential for a nucleon within the target nucleus is used as the driving term to obtain \mathcal{T}_i as solution of a Lippmann-Schwinger type equation. The inclusion of this correction, \mathcal{T}_i , corresponds to a modification of the free NN propagator, g_0 , due to the nuclear medium in order to recover the propagator G_0 , which correctly represents the propagation of the target nucleon through the nucleus. Our calculations use two different models for the mean fields, one is the nonlocal, nonrelativistic mean field potential taken from a Hartree-Fock-Bogolyubov calculation [8]. Curves based on this choice are represented by dash-dotted lines. The second choice involves a nonrelativistic reduction of the mean field potentials resulting from a Dirac-Hartree calculation based upon the σ - ω model [10]. Curves based on this choice are represented as dashed lines. Calculations using only the free NN t-matrix correspond to a truncation of Eq. (2.7) after the first term, so that

$$\tilde{t}_{0i} \approx t_{0i}^{free} . \quad (3.1)$$

Results using this truncation are included in the figures to illustrate the importance of the correction due to \mathcal{T}_i in the energy regime under discussion. The corresponding curves are

shown as solid lines.

IV. COMPARISON WITH DATA

The elastic neutron and proton elastic scattering observables [differential cross section $\frac{d\sigma}{d\Omega}$, analyzing power A_y and spin rotation function Q] are calculated for ^{12}C , ^{16}O , ^{28}Si , ^{40}Ca , ^{56}Fe , ^{90}Zr and ^{208}Pb . In all of these cases, except for ^{16}O and ^{90}Zr , neutron differential cross section data [1] exist for the natural elements along with the more extensive proton data. The carbon calculations in Fig. 1 should not be taken as seriously as the others, since it is known that carbon is a highly deformed nucleus. For a realistic calculation of carbon certain additional collective degrees of freedom need to be considered.

The overall impression is that the first order, parameter free multiple scattering predictions provide a very good representation of the data for angles below $\sim 60^\circ$, which is a very pleasant surprise. One possible partial explanation for this good agreement is that the momentum transfer for 65 MeV for $\theta = 180^\circ$ is roughly equivalent to that corresponding to $\theta = 60^\circ$ at 260 MeV. That is to say, the range of momentum transfer under observation is rather small relative to that considered at higher energies. Nonetheless, this good a description of the data is unexpected. At this low an energy, the higher order terms in the spectator expansion were expected to become important. It now appears that these terms will not be strongly structured and so will, no doubt, raise the forward cross section and fill in the sharp diffraction minima. A change in the spin structure due to higher order terms may only be apparent at large scattering angles.

In a recent publication the authors concentrated on the total cross section σ_{tot} for neutron scattering from ^{16}O and ^{40}Ca as a function of scattering energy [11]. It was found that our calculations reproduced the neutron total cross section data above ~ 100 MeV, whereas at 65 MeV the first order multiple scattering theory predictions for the total cross sections for ^{40}Ca fall short of the measured values by about $\sim 10\%$. Thus, for example, if one looked at the proton elastic differential cross section in the forward cone, one might be surprised

to see how well the data is represented by the theoretical predictions. On the other hand, it is observed that the theoretical curve for the neutron elastic differential cross section consistently falls below the data in the forward cone. The reason is that in the proton case the Coulomb effect dominates at small scattering angles and thus masks any underprediction. It may also be argued that the neutron projectile should be able to penetrate further into the nucleus than a proton projectile, due to the lack of the coulomb barrier. This may perhaps mean that for heavier nuclei, neutron scattering might be more sensitive to higher order multiple scattering effects as well as to the medium corrections used here. This is offered to illustrate the enhanced value and impact of having combined neutron and proton data sets.

The curves presented show very clearly that the inclusion of the propagator modification arising from the coupling of the struck nucleon to the residual nucleus improves the description of the data, in some cases dramatically. For neutron scattering only differential cross section data for angles up to 60 degrees are at present available. While this data is limited, a definite improvement from the propagator modification is seen. Relative to the unmodified calculation the diffraction minima systematically move to higher angles in better accord with the observation and the diffraction minima become less sharp also in accord with observation. For proton scattering, extensive data are available for $\frac{d\sigma}{d\Omega}$, A_y and Q . While there is always marked improvement in the differential cross section description due to the propagator medium modification, the effect on the spin observables A_y and Q is even more striking. For A_y at the first diffraction minima the propagator modification moves the theoretical curve closer towards the data so that for up to about 50 – 60 degrees there is a pretty good representation of the data. The effect on the Q function is even more dramatic where the medium correction shifts the curve down significantly so that the theoretical curve sits almost directly on top of the data for angles up to about 60 degrees. It appears that for Q , the propagator modification is required to obtain an excellent agreement with the data, and it is further remarkable that this is the case for all nuclei under consideration. The theoretical predictions for the heavier elements ^{90}Zr and ^{208}Pb are not as good as for the lighter nuclei, but the dramatic effect observed for the Q function remains. The effect

of the propagator modification on the spin rotation is slightly larger for neutron scattering than for protons and in Figs. 4-7 this difference is even larger for both Q and A_y . The good description of the spin observables independent of the mass of the nucleus may be taken as evidence that at these low energies the scattering process is generally completely surface dominated, and by construction our theoretical approach captures the effect of the coupling of the struck target nucleon to the mean field of the residual nucleus.

All the nuclei under consideration are even-even nuclei. However, in a shell model sense they are mostly not ‘spin-saturated’, and so one might expect that all Wolfenstein parameters in the NN t-matrix to contribute to the optical potential. The remarkable description of the data which is obtained here based on only A and C suggests that such effects are small. This may give information concerning the structure of the target, but in the present stage it would be premature to test sensitivities to the correlation structure of the target.

V. SUMMARY AND CONCLUSION

The success of our calculations at higher energies [3,11] have emboldened us to venture toward energies lower than previously considered. Neutron and proton elastic scattering observables are calculated in first order multiple scattering theory in a parameter free fashion for a number of even-even spin zero targets at 65 MeV. Even at this low energy a good description of the data is obtained. It is observed that the propagator modification due to the coupling of the struck nucleon to the residual nucleus invariably brings the theoretical results into closer agreement with observation.

The availability of both neutron and proton scattering data at the same energy is especially valuable. At this energy we find that our theoretical predictions consistently underpredict the neutron differential cross section in the forward direction; whereas, in the corresponding proton differential cross section, Coulomb effects mask this underprediction. This illustrates the enhanced value and impact of having available combined neutron and proton data sets.

ACKNOWLEDGMENTS

The authors would like to thank R.W. Finlay and J. Rapaport for many discussions concerning this work. The computational support of the the Ohio Supercomputer Center under Grants No. PHS206 and PDS150 is gratefully acknowledged. This work was performed in part under the auspices of the U. S. Department of Energy under contracts No. DE-FG02-93ER40756 with Ohio University, DE-AC05-84OR21400 with Martin Marietta Energy Systems, Inc., and DE-FG05-87ER40376 with Vanderbilt University. This research has also been supported in part by the U.S. Department of Energy, Office of Scientific Computing under the High Performance Computing and Communications Program (HPCC) as a Grand Challenge titled “The Quantum Structure of Matter”.

REFERENCES

- [1] E. L. Hjort, F. P. Brady, J. L. Romero, J. R. Drumond, D. S. Sorenson, J. H. Osborne and B. McEachern, Phys. Rev. **C 50**, 275 (1994).
- [2] C.R. Chinn, Ch. Elster, and R.M. Thaler, Phys. Rev. **C48** 2956 (1993).
- [3] C. R. Chinn, Ch. Elster and R. M. Thaler, Phys. Rev. **C 44**, 1569 (1991).
- [4] T. Cheon, Ch. Elster, E. F. Redish, and P. C. Tandy, Phys. Rev. **C41** (1990), 841.
- [5] R. Crespo, R. C. Johnson, and J. A. Tostevin, Phys. Rev. **C41** (1990), 2257.
- [6] A. Picklesimer, P. C. Tandy, R. M. Thaler, and D. H. Wolfe, Phys. Rev. **C 30**, 1861 (1984).
- [7] R. Machleidt, K. Holinde, and Ch. Elster, Phys. Rep. **149**, (1987).
- [8] See for example J.F. Berger, M. Girod, and D. Gogny, Nucl. Phys. **A502**, 85c (1989); J.P. Delaroche, M. Girod, J. Libert and I. Deloncle, Phys. Lett. **B232**, 145 (1989).
- [9] J.F. Berger, M. Girod, and D. Gogny, Comput. Phys. Commun. **63**, 365 (1991).
- [10] Horowitz and B. Serot, Nucl. Phys **A368**, 503 (1981).
- [11] C. R. Chinn, Ch. Elster, R. M. Thaler, and S. P. Weppner, submitted to Phys. Rev. C.
- [12] I. Sick, J. B. Bellicard, J. M. Cavedon, B. Frois, M. Huet, P. Leconte, P. X. Ho, and S. Platchkov, Phys. Lett. **88B**, 245 (1979); B. Frois, J.B. Bellicard, J.M. Cavedon, M. Huet, P. Leconte, P. Ludeau, A. Nakada, and P.X. Ho, Phys. Rev. Lett. **38**, 152 (1977).
- [13] S. Kato et al., Nucl. Inst. and Meth. **169**, 589 (1980); H. Sakaguchi et al., J. Phys. Soc. Jpn. Suppl. 55, 61 (1986).
- [14] H. Sakaguchi, M. Nakamura, K. Hatanaka, A. Goto, T. Noro, F. Ohtani, H. Sakamoto, H. Ogawa, and S. Kobayashi, Phys. Rev. **C 26**, 944 (1982).

FIGURES

FIG. 1. The differential cross section, analyzing power and spin rotation functions are shown for elastic nucleon scattering from ^{12}C . The left three panels show elastic neutron scattering, while the right three panels are for proton scattering. The neutron data are from Ref. [1], while the proton data are from Ref. [13]. In all cases, the solid line corresponds to a calculation of the first order optical potential based on the free NN t-matrix from the full Bonn model [7] as input. The dashed and dash-dotted lines include the propagator modification due to the nuclear mean field. For the dash-dotted curve a Hartree-Fock-Bogolyubov [8] is used, for the dashed curve a Dirac-Hartree mean field [10].

FIG. 2. The same as Fig. 1, except for ^{16}O and the elastic proton scattering data are from Ref. [14].

FIG. 3. The same as Fig. 1 except for ^{26}Si and the elastic proton scattering data are from Ref. [14].

FIG. 4. The same as Fig. 1 except for ^{40}Ca and the elastic proton scattering data are from Ref. [14].

FIG. 5. The same as Fig. 1 except for ^{56}Fe and the elastic proton scattering data are from Ref. [14].

FIG. 6. The same as Fig. 1 except for ^{90}Zr and the elastic proton scattering data are from Ref. [14].

FIG. 7. The same as Fig. 1 except for ^{208}Pb and the elastic proton scattering data are from Ref. [14].

This figure "fig1-1.png" is available in "png" format from:

<http://arxiv.org/ps/nucl-th/9410029v1>

This figure "fig1-2.png" is available in "png" format from:

<http://arxiv.org/ps/nucl-th/9410029v1>

This figure "fig1-3.png" is available in "png" format from:

<http://arxiv.org/ps/nucl-th/9410029v1>

This figure "fig1-4.png" is available in "png" format from:

<http://arxiv.org/ps/nucl-th/9410029v1>

This figure "fig1-5.png" is available in "png" format from:

<http://arxiv.org/ps/nucl-th/9410029v1>

This figure "fig1-6.png" is available in "png" format from:

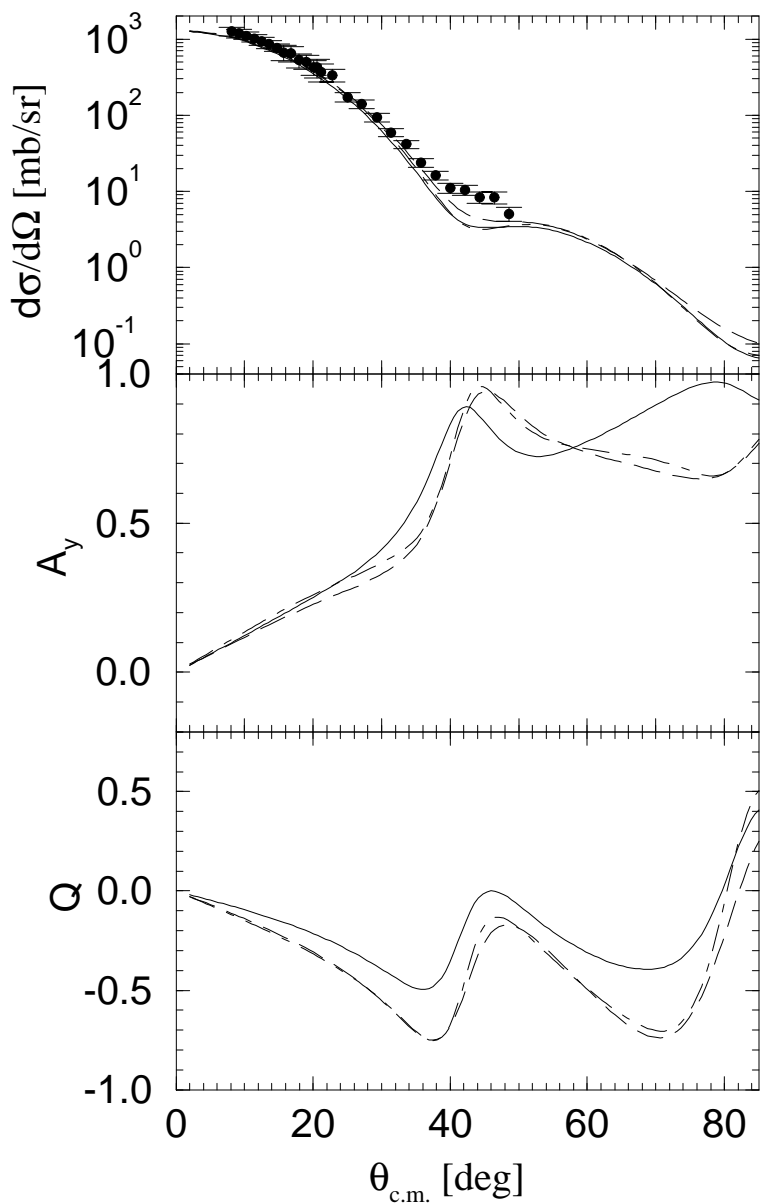
<http://arxiv.org/ps/nucl-th/9410029v1>

This figure "fig1-7.png" is available in "png" format from:

<http://arxiv.org/ps/nucl-th/9410029v1>

Figure 1

^{12}C , neutron scattering



^{12}C , proton scattering

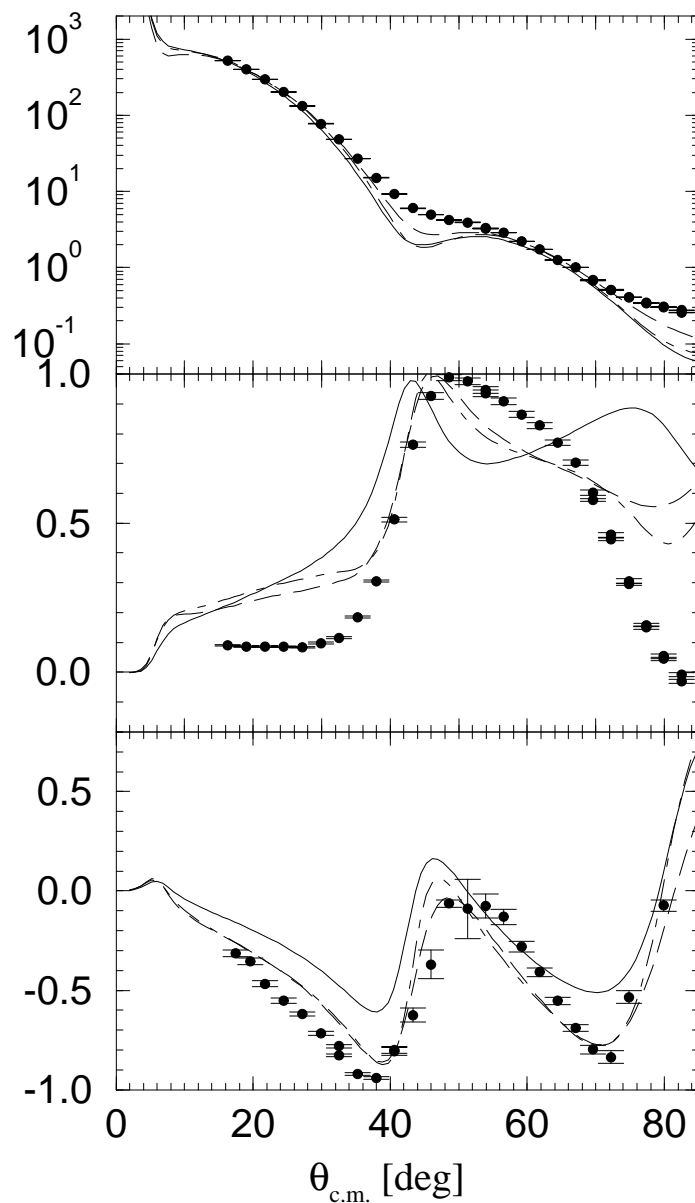
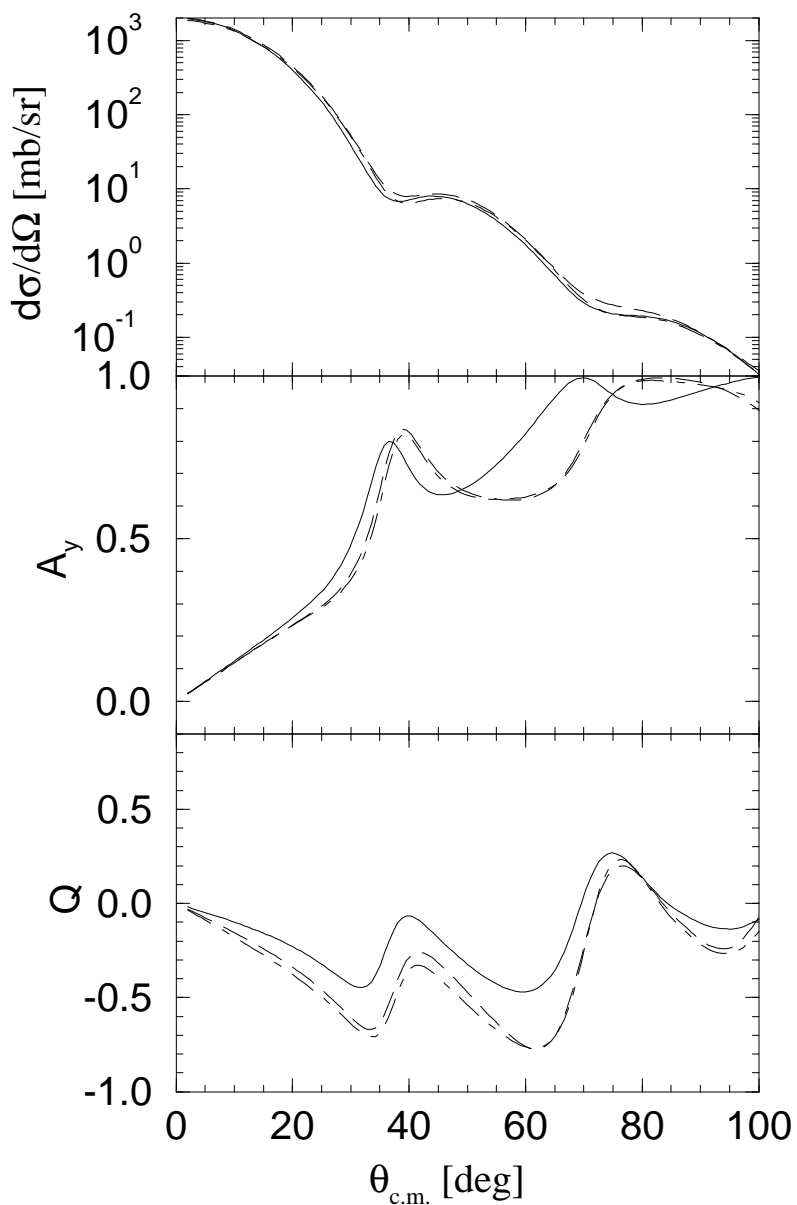


Figure 2

^{16}O , neutron scattering



^{16}O , proton scattering

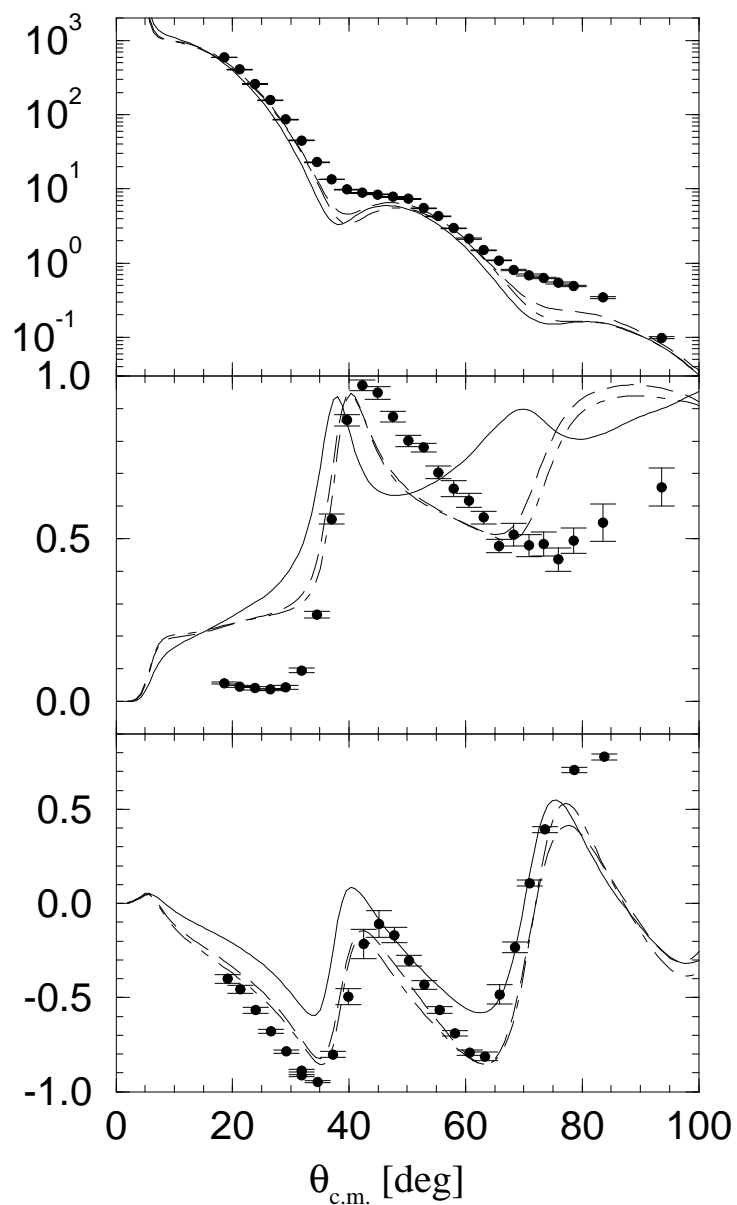
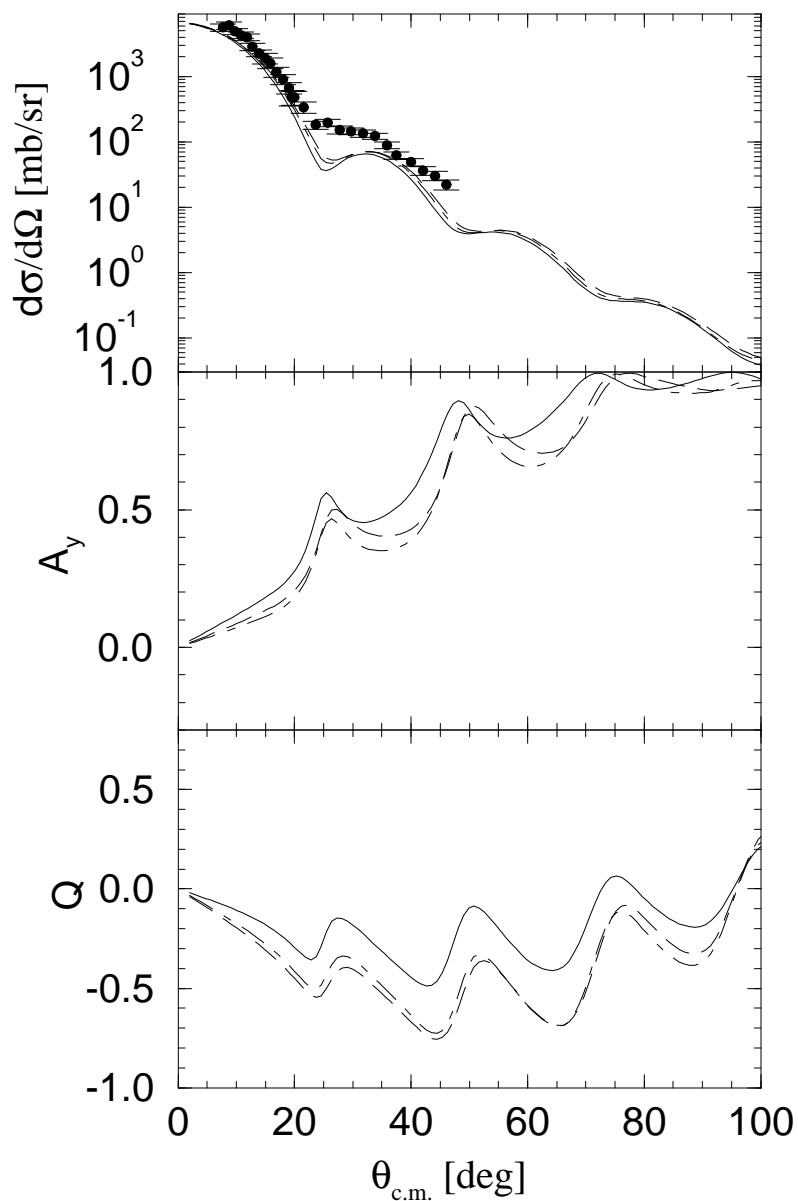


Figure 4

^{40}Ca , neutron scattering



^{40}Ca , proton scattering

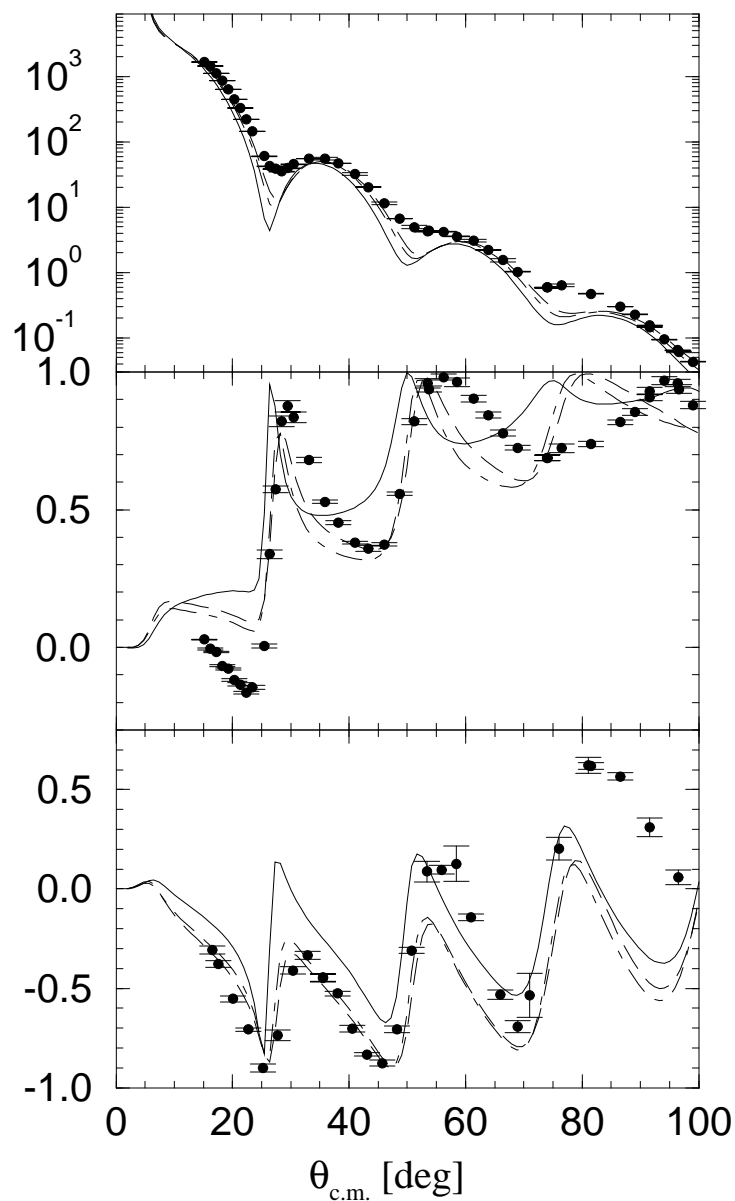
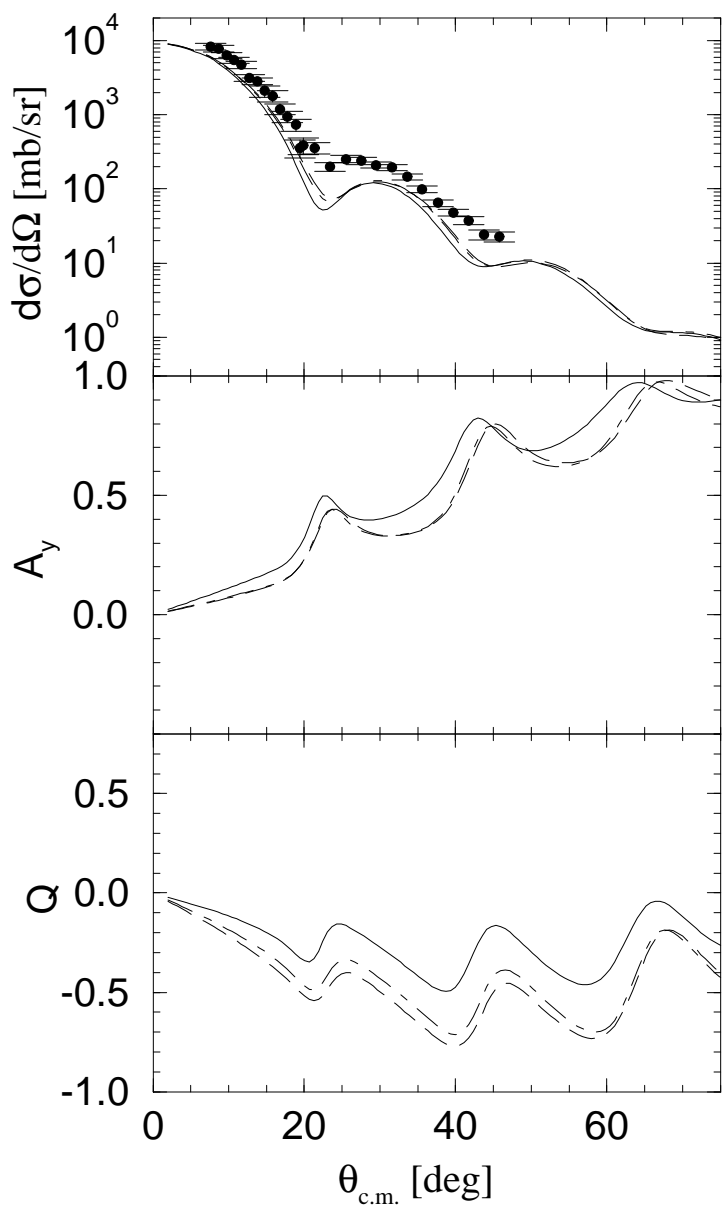


Figure 5

^{56}Fe , neutron scattering



^{56}Fe , proton scattering

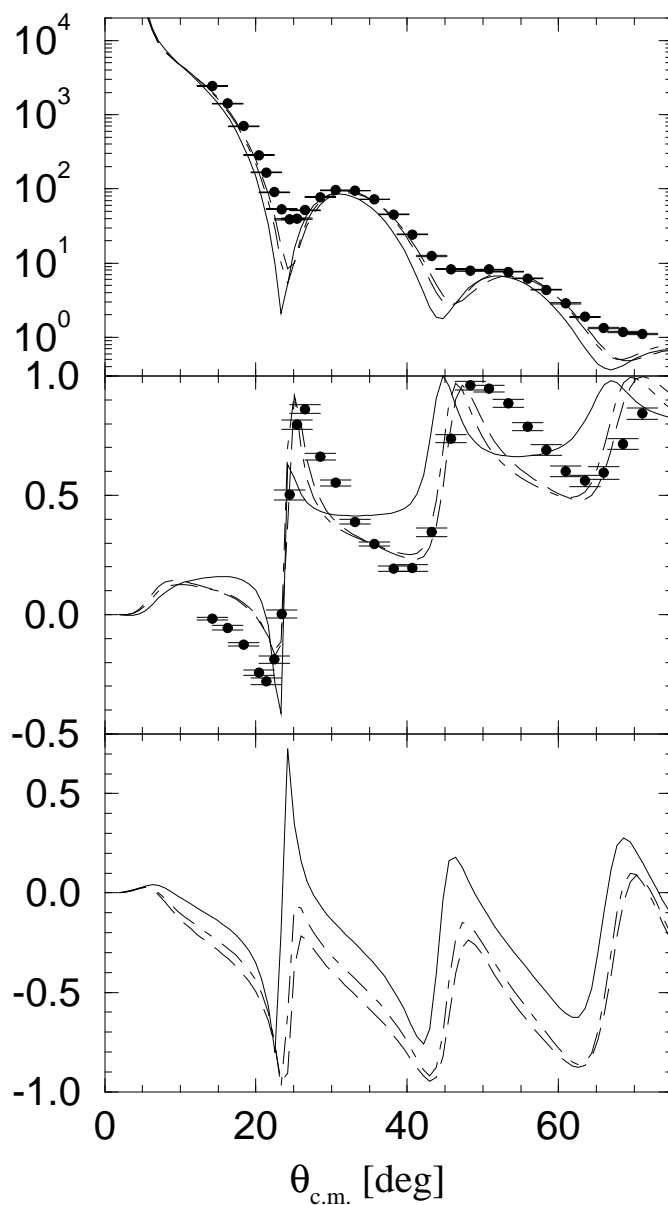
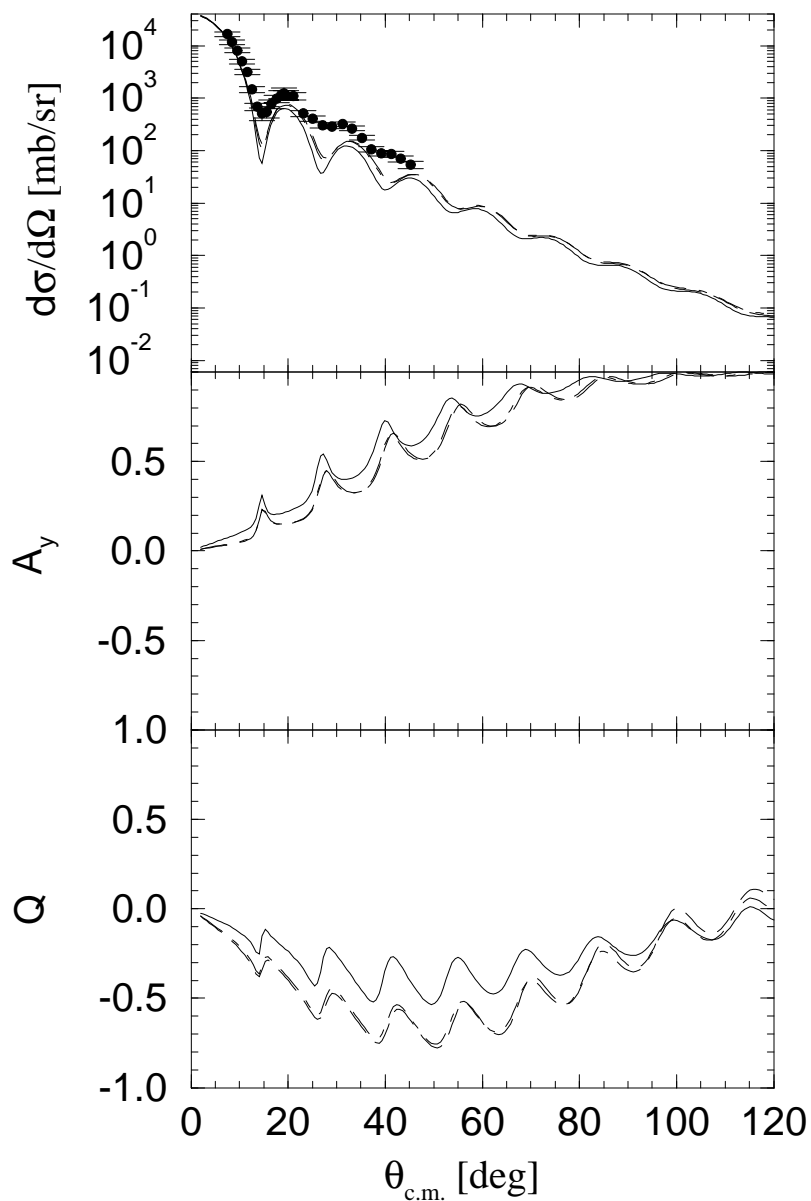


Figure 7

^{208}Pb , neutron scattering



^{208}Pb , proton scattering

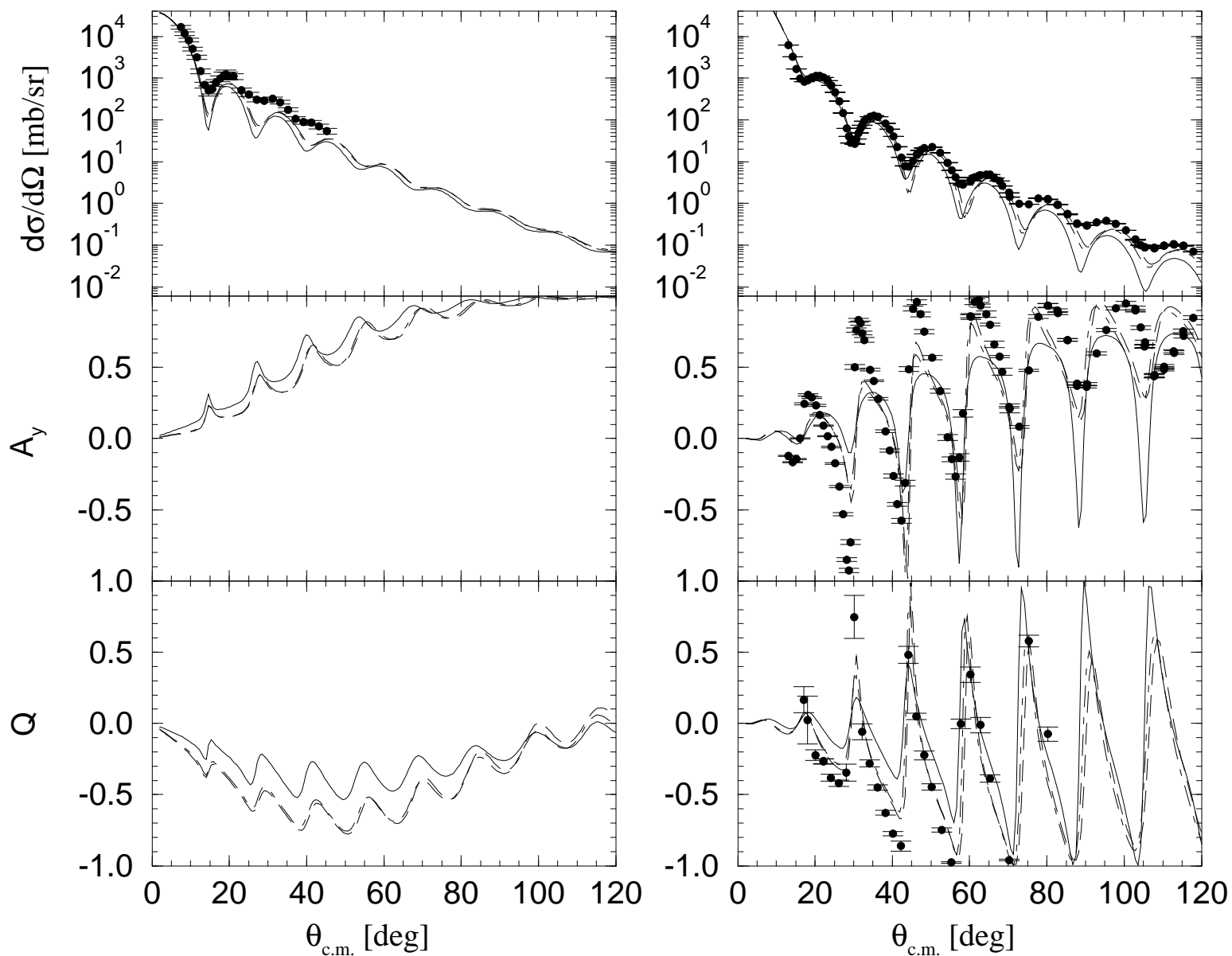
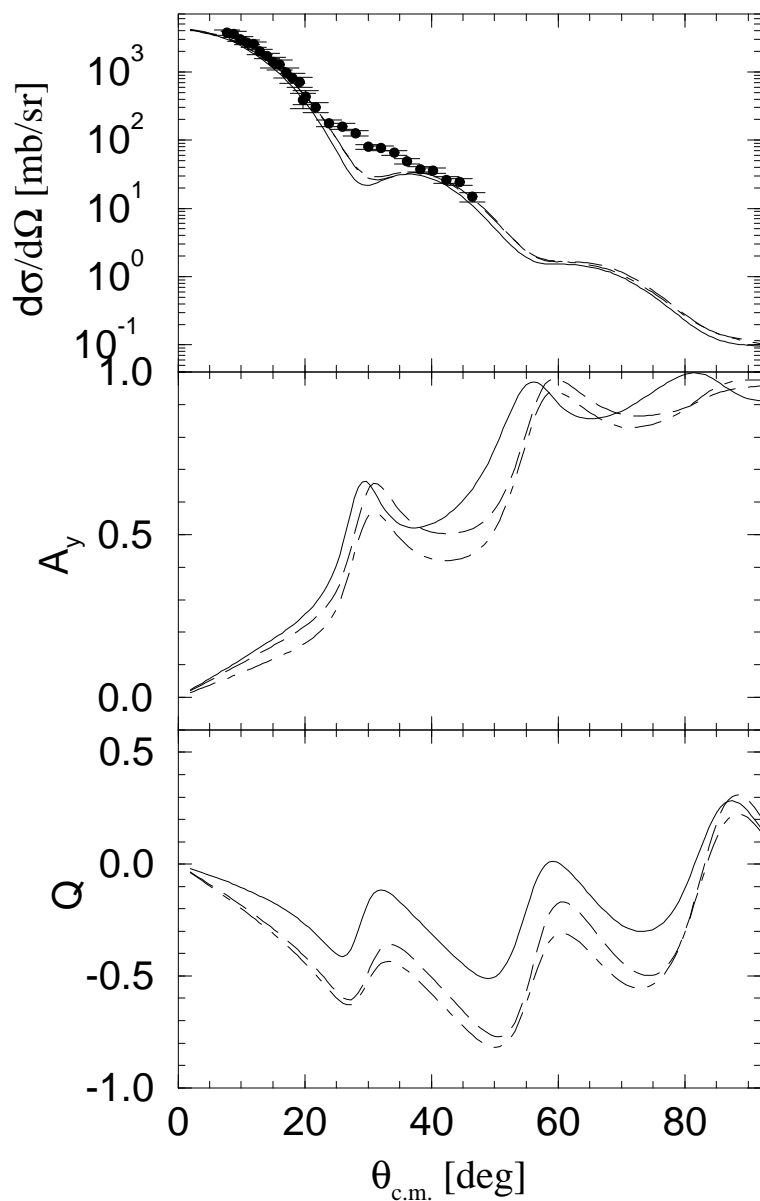


Figure 3

^{28}Si , neutron scattering



^{28}Si , proton scattering

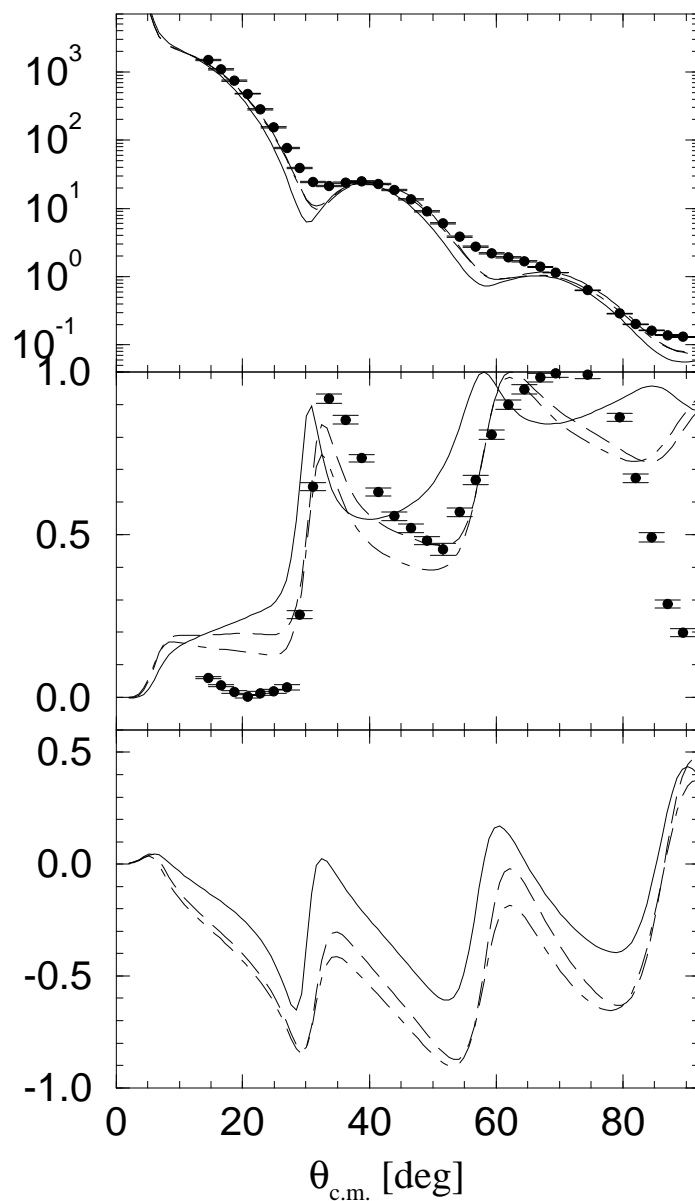
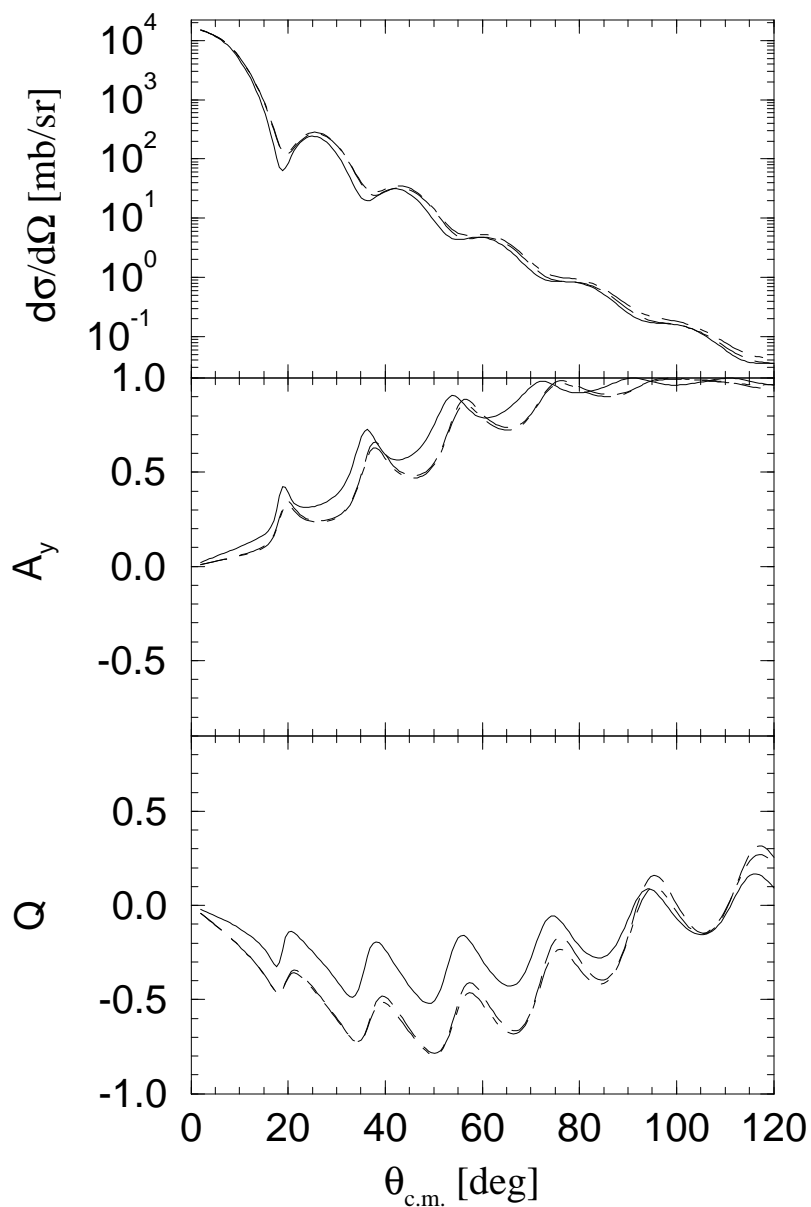


Figure 6

^{90}Zr , neutron scattering



^{90}Zr , proton scattering

